Indian Journal of Geo Marine Sciences
Vol. 54 (04), April 2025, pp. 175-182
DOI: 10.56042/ijms.v54i04.16358

Research Article

The ocean heat content in the northwest Indian Ocean region

I A Maiyza, T M El-Geziry*, A S Dabbous & H I Maiyza
National Institute of Oceanography and Fisheries (NIOF), Cairo, Egypt
*[E-mail: tarekelgeziry@yahoo.com]

Received January 12, 2025; revised 04 April 2025

Ocean Heat Content (OHC) is crucial for understanding ocean dynamics. The Northwest Indian Ocean (NWIO) region, comprising the Southern Red Sea, the Gulf of Aden, the Arabian Sea, and the Equatorial North West Indian Ocean, is affected by various phenomena, such as upwelling, heat waves, and multi-layer exchange between the Red Sea and the Gulf of Aden. The spatial and temporal variability of these factors affects upper-layer OHC. OHC in the NWIO region has rarely been studied earlier. Therefore, this work would be beneficial in filling the knowledge gap and understanding the OHC of this region. The study displays the horizontal distributions of monthly OHC and yearly signal amplitudes, calculated as the difference between maximum and minimum values across all months, along with the monthly mean OHC patterns in the upper 100 m and 300 m layers of the NWIO, based on the available historical seawater temperature and salinity data from the World Data Centre (WDC-A, Washington D.C.), WDC-B (Moscow) and the Egyptian National Oceanographic Data Centre (ENODC). The region exhibited a similar pattern of monthly average OHC in the upper 100 and 300 m layers, except within the Equatorial North West Indian Ocean zone. In addition, the lower layer within the Red Sea exhibited a different pattern during the winter and transitional months. The NWIO region demonstrated homogeneous annual OHC signal amplitudes, except for the Arabian Sea, which has the highest annual amplitude at both layers.

[**Keywords**: Annual signal amplitudes, Arabian Sea, Northwest Indian Ocean, Ocean heat content, Red Sea]

Introduction

The Northwest Indian Ocean (NWIO) region comprises many basins. The Arabian Sea is one of the most important basins in the NWIO, bordered on the north by Pakistan, Iran, and the Gulf of Oman, on the west by the Gulf of Aden and the Arabian Peninsula, on the southeast by the Laccadive Sea and the Maldives, and on the southwest by Somalia. The NWIO connects to the Arabian Sea adjacently, and to the Red Sea and the Arabian Gulf, marginally. The Gulf of Aden in the northwest meets the Red Sea via the Bab El-Mandeb Strait, and the Gulf of Oman in the northeast is connected to the Arabian Gulf through the Hormuz Strait[1,2]. The Arabian Sea is an important source of biogeochemical ocean-atmosphere exchanges, which are essential for controlling the chemical composition of the atmosphere and the climate of the world[3]. In addition, the Arabian Sea has been a significant maritime trade route since the time of coastal sailing vessels. In general, the NWIO not only provides fishing and oil resources, but it also serves as a significant shipping route between Southeast Asia and Europe, and other areas worldwide. This region stretches from the African Coast at 40° E to 60° E within the Indian Ocean and from the Equator to 20° N, as shown in Figure 1.

The NWIO region is influenced by strong monsoon regimes[4-8], upwelling[9-12], marine heat waves[13,14], and water exchange with the Red Sea[15-18]. Moreover, the exchange between the Arabian Gulf and the NWIO has been investigated earlier in a few studies[18-21]. Although the yearly transit of discharges from the Red Sea and Arabian Gulf is minor (< 0.4 Sv), their high salinity has a significant impact on the Indian Ocean's hydrography at the thermocline level[22], and extends over a wide surface area of the Northern Indian Ocean[18,20]. Generally speaking, the Red Sea shows stronger seasonal variability in the observed outflows than the Arabian Gulf[18,22]. Natural climatic variability, such as the El Niño-Southern Oscillation (ENSO), Indo-Pacific warm pool, and Indian Ocean Dipole (IOD) impact the NWIO warming on interannual and decadal timescales[23-25]. The surface and subsurface water temperatures of the Indian Ocean, particularly the Northern Indian Ocean (NIO), have an important role in regulating monsoon patterns and cyclonic activity across the Indian subcontinent[26]. All of these phenomena affect OHC in the upper water layer in this area. OHC plays an essential role in the ocean dynamics. The surface layer of the Indian Ocean exhibits wide spatiotemporal variations in its

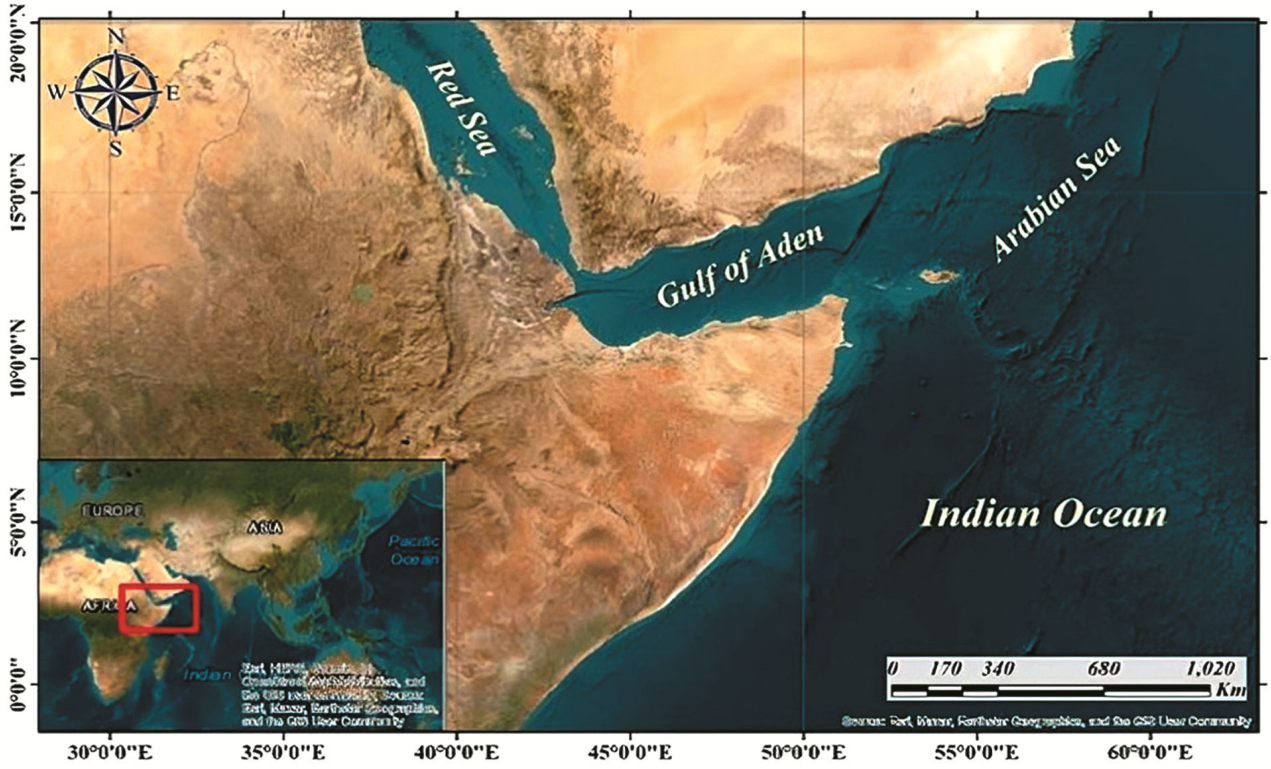

Fig. 1 — Northwest Indian Ocean (NWIO) region (Size = 6.92 inch)

OHC. The regular formation of Sea Surface Temperature Anomalies (SSTA) in the NWIO (same present area of interest) was previously studied by Maiyza & Mohamed[27]. The variability of heat and salt storage in the upper 1000 m of the Indian Ocean was investigated, and the Indian Ocean dipole mode is shown to be essential to the Equatorial North West Indian Ocean OHC variability[28]. Gnanaseelan *et al.*[29] simulated the Sea Surface Temperature (SST) and upper OHC in the North Indian Ocean. On the other hand, Vaid *et al.*[30] computed Sea Surface Height Anomalies (SSHA) derived from the Topex /Poseidon (T/P) satellite over the North Indian Ocean. The annual OHC of the Arabian Sea was examined by Naganamani *et al.*[31]. Results of recent research revealed an exponential increase in the occurrence of marine heatwaves in the Northern Indian Ocean associated with an increasing mean surface temperature[32]. Results also indicated that subsurface temperatures are also increasing rapidly over the Arabian Sea[32]. Only a few studies have investigated OHC in the Northwest region of the Indian Ocean. Most of these studies focused on the variability of OHC in the upper layer using altimetry images data and modelling. Hence, the current study would be beneficial in filling up the knowledge gap about the OHC in the northern region of the Indian Ocean by examining its monthly horizontal distribution, the horizontal distribution of the annual signal amplitudes (calculated as the difference between maximum and minimum values across all months), and the annual trend of monthly mean OHC in the upper 100 m and 300 m layers of the NWIO, including the Arabian Sea, Gulf of Aden, Southern Red Sea, and the Equatorial North West Indian Ocean.

Materials and Methods

The Study area

The area of investigation was divided into four regions. These regions were made at the chosen grids, as shown in Figure 2: the first region is the Southern Red Sea (Grids 1 – 3), the second is the Gulf of Aden (Grids 4 – 6), the third is the Arabian Sea (Grids 7 – 10), and the fourth region is the Equatorial North West Indian Ocean (Grids 11 – 16).

Methodology and data analysis

The mean monthly seawater temperature and salinity, for each grid and standard hydrographic level, of the upper 300 m layer in the area of interest

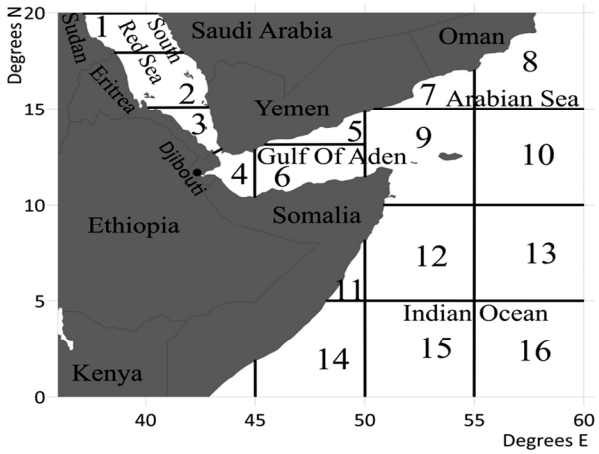

Fig. 2 — Study area: South Red Sea region (Grids 1 – 3); Gulf of Aden region (Grids 4 – 6); Arabian Sea region (Grids 7 – 10); and Equatorial North West Indian Ocean region (Grids 11 – 16) (Size = 3.33 inch)

were computed from the historical data files available from the World Data Centre (WDC) WDC-A (Washington D.C.), WDC-B (Moscow), and the Egyptian National Oceanographic Data Centre (ENODC). The temperature datasets from the various sources spanned the period of 1933 – 2008 (76 years) with diverse density in each grid of interest. The accuracy of records from both WDC and ENODC was 0.1 °C. The study area exhibits two seasons: winter (from November to March), and summer (from June to October). April and May are two season-transitional months.

The data were measured/computed at standard depths (0 – 100 m & 0 – 300 m). To obtain higher-quality hydrographic data, the data were primarily subjected to objective analysis prior to any calculation. It is noteworthy that only a few observations were rejected due to poor quality, perhaps due to personal, instrumental, and/or location errors. Using the above randomly distributed temperature data, the values at each grid centre were calculated for each month. Table 1 summarises the statistical measures of the recorded annual temperature at the 100- and 300-m layers.

As seawater temperature is the key driver of the calculated OHC, the salinity values in the present work were considered constant, ranging from 10 to 43 psu.

The seawater density (ρ kg/m^3) was calculated based on the sigma-t values, which were calculated based on temperature records and salinity limits, using the standard equations[33]:

$$\text{Sigma-t} = 28.152-(0.0735T)-(0.00469T^2)+((0.802-0.002T)(S-35)) \quad \ldots (1)$$

$$\rho = \text{sigma-t} + 1000 \text{ kg/m}^3 \quad \ldots (2)$$

Table 1 — Statistical measures of the recorded annual temperature at the two layers of interest

	0 – 100 m original data		0 – 300 m original data	
	Temperature	Year	Temperature	Year
Number of values	83459	83459	217230	217230
Minimum	13.5	1933	10.4	1933
Maximum	36.4	2008	36.5	2008
Mean	24.3		19.6	
Standard deviation	3.5		5.0	

Ocean Heat Content (OHC) at any grid centre is calculated according to Levitus[34,35], relative to 0 °C:

$$OHC = \int_0^z \rho C_p T dz \quad \ldots (3)$$

$$C_p = 4186 * \{[1.0049 - 0.001621\ S + (3.5261 * 10^{-6}\ S^2) - [(3.2506 - 0.14795\ S + 7.7765 * 10^{-4}\ S^2) * 10^{-4}\ T] + [(3.8103 - 0.12084\ S + 6.121 * 10^{-4}\ S^2) * 10^{-6}\ T^2]\} \ldots (4)$$

Where, *OHC* is the Ocean Heat Content (J/m^2), ρ is the density of the seawater (kg/m^3), C_p is the specific heat capacity (J /kg°C), *T* is the seawater temperature (°C), *S* is the seawater salinity, and *z* is the depth (m).

Results

Monthly climatological ocean heat content (1933-2008)

The pattern was determined by calculating the mean monthly OHC data for each region. Figure 3 displays the mean monthly OHC for the upper 100 m (upper panel) and 300 m (lower panel) layers. In the 100 m layer, the monthly average OHC showed similar patterns across different regions, with a dramatic drop in OHC from May to June persisting throughout the summer months, except in the Equatorial North West Indian Ocean. In the 300 m layer, the monthly average OHC increased in the southern Red Sea region relative to the other three regions throughout the study period, except during the summer months. This sub-region solely showed a clear increase in its OHC from September to November.

Spatial distribution of monthly climatological ocean heat content

Figures 4 and 5 show the OHC (per unit area) in the study area, calculated within the upper water column from the sea surface to depths of 100 and 300 m, respectively, during different months. The amount of OHC varied spatially between 6×10^9 and 14×10^9 J/m^2 in the upper 100 m. The minimum value was observed in the Arabian Sea (grid 10) during summer in June, whereas the maximum value was found in the Equatorial North West Indian Ocean (grid 14) during the transitional month of April. For the upper 300 m,

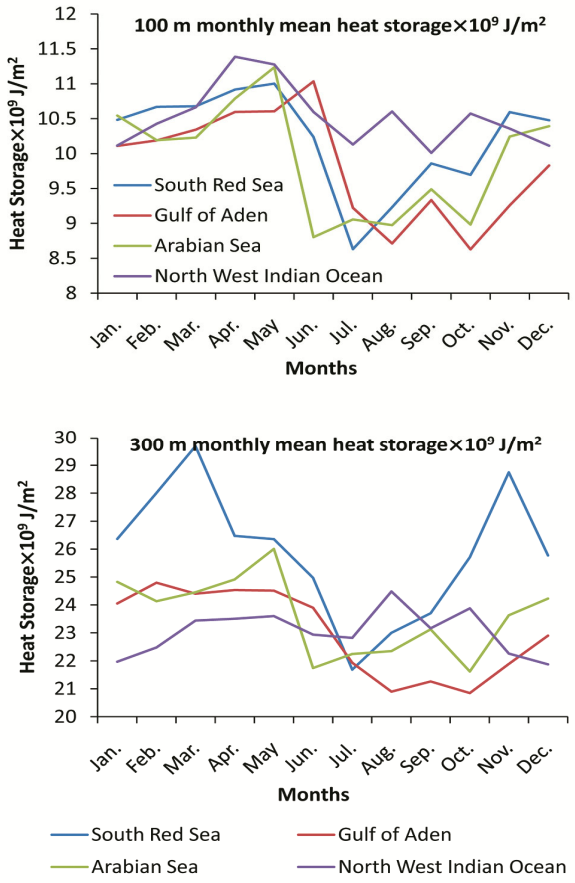

Fig. 3 — Average monthly ocean heat content time series at 100 m and 300 m during the study period

the amount of OHC varied between 17×10^9 and 29×10^9 J/m^2. The minimum value was also observed in the Arabian Sea (grid 10) in June, similar to as occurred in the 100 m layer, whereas the maximum value was observed in the South Red Sea in March.

During winter, the OHC ranged between 9.4×10^9 and 11×10^9 J/m^2 in the 100 m layer. The minimum value was observed in the Gulf of Aden (grid 6) in December, whereas the maximum value was found in the Equatorial North West Indian Ocean (grid 16) in March. In addition, Figure 4 depicts a slight increase in the amount of OHC toward the open sea, except in grid 15 within the Equatorial North West Indian Ocean in January and April. For the 300 m layer, the amount of OHC varied between 21×10^9 and 29×10^9 J/m^2. The minimum value was observed in the Equatorial North West Indian Ocean (grid 16) in January, whereas the maximum value was found in the South Red Sea in March. In the 300 m layer, the OHC varied across the diverse sub-regions in the study area.

During transitional months (April and May), the amount of OHC varied between 10.5×10^9 and 12.4×10^9 J/m^2 in the 100 m layer, whereas for the 300 m layer, it varied between 23×10^9 and 28×10^9 J/m^2, as shown in Figure 4. The minimum value was observed in the Equatorial North West Indian Ocean (grid 13) in April, whereas the maximum value was observed in the Equatorial North West Indian Ocean (grid 14) in

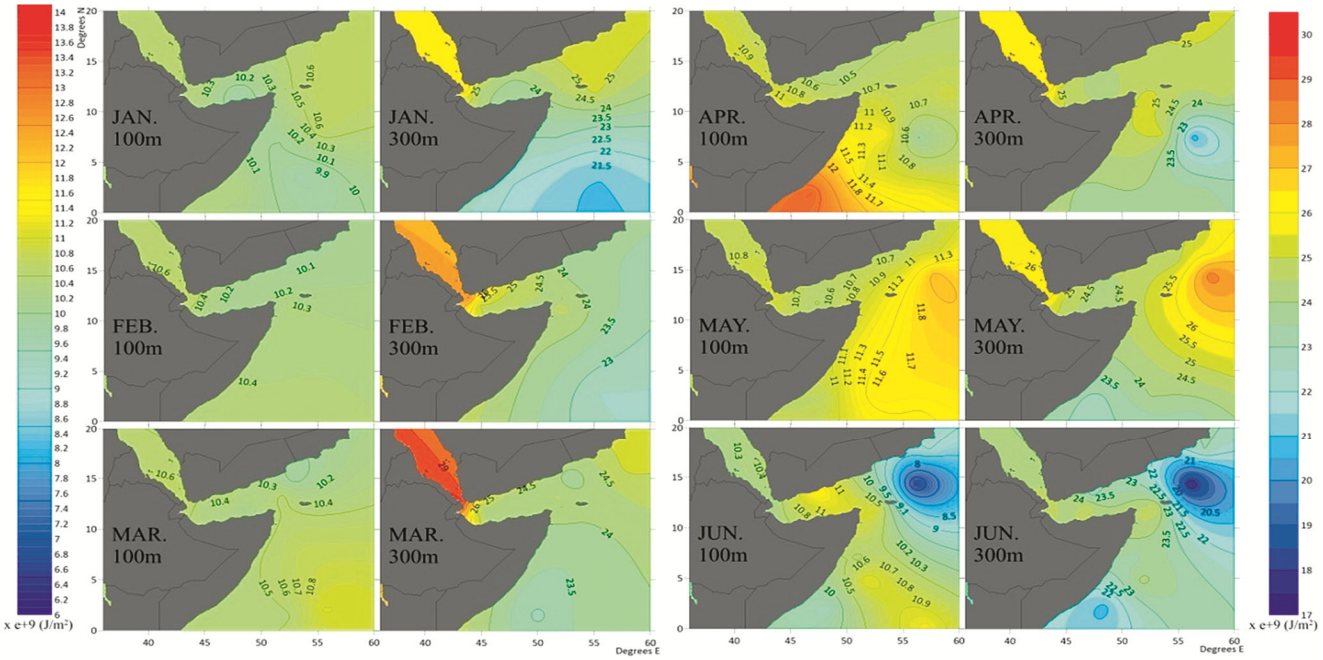

Fig. 4 — The monthly Ocean Heat Content (OHC) at 100 m and 300 m depth (January – June) (Size = 6.92 inch)

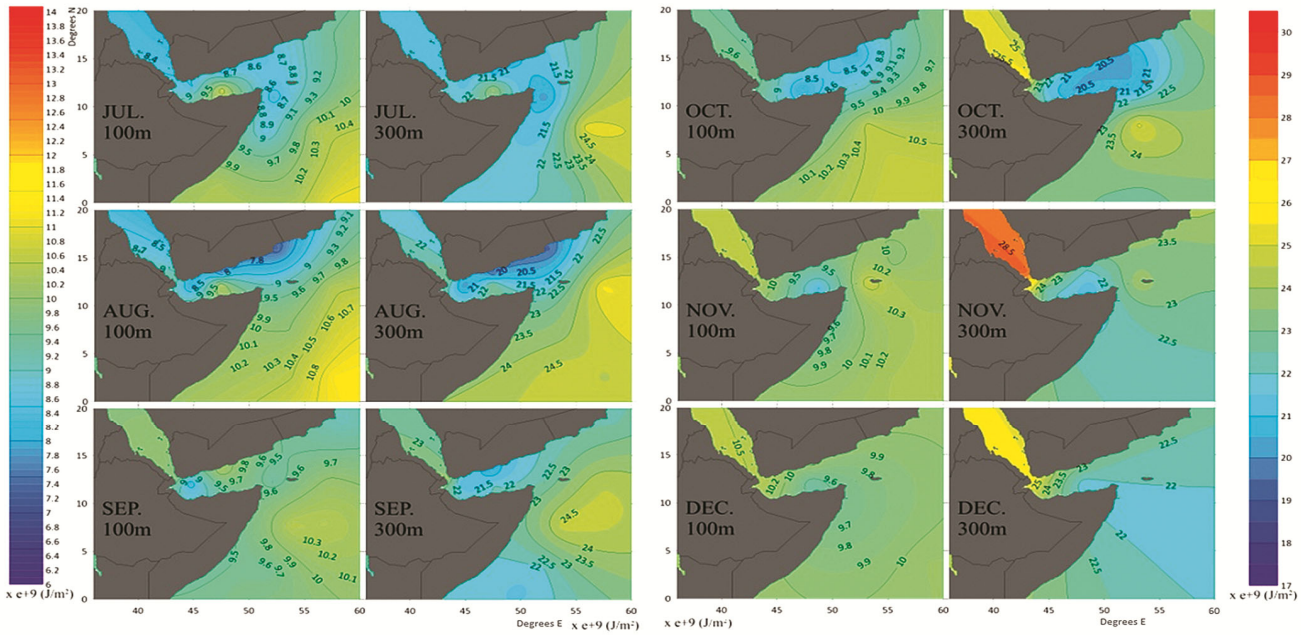

Fig. 5 — The monthly Ocean Heat Content (OHC) at 100 m and 300 m depth (July – December) (Size = 6.92 inch)

May for the 100 m layer. For the upper 300 m, the minimum OHC value was observed in the Equatorial North West Indian Ocean in April, whereas the maximum values were observed in the Arabian Sea (grid 10) in May. The upper 100 m and 300 m layers showed the similar OHC pattern.

During the summer (June to October), the OHC in the study area exhibited a different behaviour. Results revealed that the minimum values occurred close to the coast, and then increased slightly toward the open sea, reaching their maximum values in the Equatorial North West Indian Ocean. In addition, the upper 100 m layer and the 300 m layer showed the same OHC pattern as observed during the transitional months. The heat content varied between 6.5×10^9 and 11×10^9 J/m^2 in the 100 m layer. For the upper 300 m, the OHC varied from 19.5×10^9 to 25×10^9 J/m^2. The minimum value was observed within the Arabian Sea (grid 10) in June for the two layers, whereas the maximum was found in the Equatorial North West Indian Ocean (grid 16) in August for the 100 m layer, and in July and August for the 300 m layer in the Equatorial North West Indian Ocean (grid 13).

Ocean heat content signal amplitudes distribution

The difference between the monthly maximum and minimum OHC values for each grid was used to calculate the OHC signal amplitudes. The horizontal distribution of the signal amplitudes for each grid for the upper 100 m and 300 m layers is shown in Figure 6. This varied between 0.6×10^9 and 5.8×10^9 J/m^2 and between 3×10^9 and 11×10^9 J/m^2 for the upper 100 m and 300 m layers, respectively. Only grid 10 in the Arabian Sea had the highest value at both layers, while grid 13 in the Equatorial North West Indian Ocean had the lowest value in the upper 100 m layer. For the upper 300 m layer, three grids had the lowest values (grid 8 in the Arabian Sea and grids 14 and 16 in the Indian Ocean at the Equator).

Discussion

Numerous phenomena, including upwelling, marine heat waves, and Red Sea-Gulf of Aden exchange have an impact on the Northwest Indian Ocean (NWIO) region. Ocean Heat Content (OHC) in the upper layer in this region is affected by all of these phenomena. Additionally, the OHC is generally crucial to the dynamics of the ocean.

In this study, the behaviour of monthly variations of the mean OHC in the upper 100 m and 300 m layers of the NWIO was examined along with the horizontal distributions of monthly OHC and OHC signal amplitudes.

In the upper 100 m layer, the monthly mean OHC showed a similar pattern of variation across all regions, except in the Equatorial North West Indian. In the lower 300 m layer, the climatological OHC is higher in the Red Sea across months, which may be attributed to water exchange between the Red Sea and the Gulf of Aden through the Bab El-Mandeb Strait. This is in

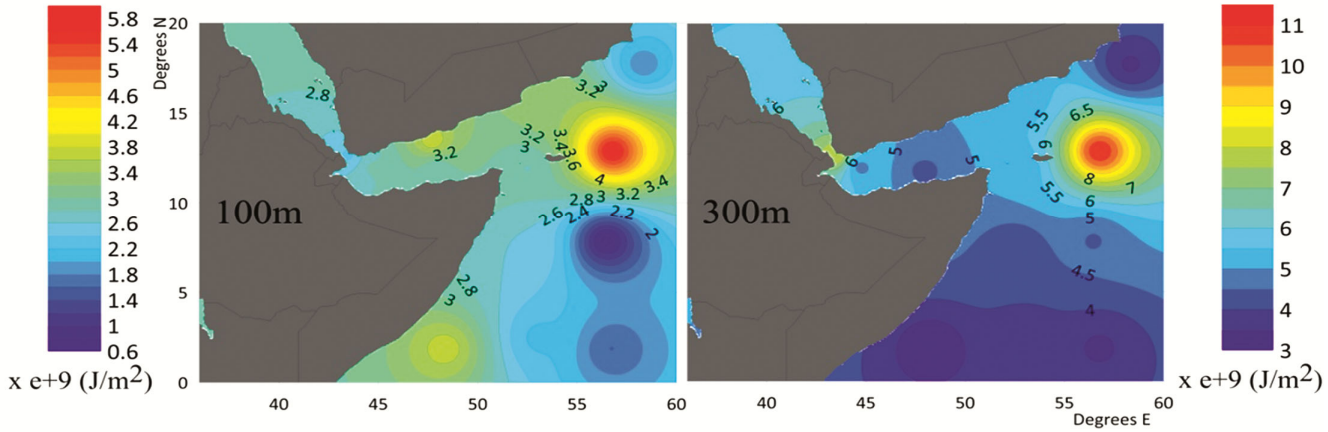

Fig. 6 — Annual amplitude of Ocean Heat Content (OHC) at 100 m and 300 m during the study period (Size = 6.92 inch)

agreement with the results of Maiyza & Mohamed[27]. Furthermore, the climatological OHC showed distinct patterns of variation at the two layers of interest throughout the seasons, except during summer. This finding agrees with those of Maillard & Soliman[15], Smeed[16], and Sofianos & Johns[17], who showed that during the summer, the OHC decreased due to the colder and thicker intermediate water of the Indian Ocean inflowing to the Red Sea between 80 and 120 dbar. Also, the temperature and salinity distributions are extremely homogenous below the sill depth (137 m) throughout the four seasons of the year[15-17].

During all months, the amount of OHC increased slightly toward the open sea in the Equatorial North West Indian Ocean, except in June for the upper 100 m layer. The thermal properties of each area within the NWIO during the winter monsoon were precisely displayed by the OHC values for the 300 m layer. During summer and transitional months, the upper 100 m and the lower 300 m layers showed the same OHC patterns.

The amount of OHC ranged between 6×10^9 and 14×10^9 J/m^2 in the upper 100 m. For the 300 m layer, the amount varied between 17×10^9 and 29×10^9 J/m^2. The minimum OHC value observed in the Arabian Sea in June in the upper 100 m and lower 300 m depth layers may be attributed to upwelling in the Arabian Sea during the summer season[11]. The maximum OHC was found in the Equatorial North West Indian Ocean in April for the upper 100 m layer. Also, there was a high ocean heat content value in the Arabian Sea in May, which might be associated with the occurrence of Marine Heat Waves (MHWs) during the pre-monsoon and summer monsoon seasons[13]. Chatterjee *et al.*[13] reported the MHW characteristics for the Arabian Sea over the period 1982-2019. They discovered that the majority of the marine heatwave days recorded annually occur during the pre-monsoon and summer monsoon seasons, with over 60 % of heatwave days in the Arabian Sea occurring during these two seasons. The strongest tendency during the pre-monsoon season is mainly restricted to the western boundary of the Arabian Sea along the coasts of Arabia and Somalia, the northern Arabian Sea along the coast of Pakistan, and the northwest coast of India. The western Arabian Sea exhibits no discernible trend in heatwave days during the summer monsoon. Nonetheless, the SST rapidly cools near the western boundary of the Arabian Sea by late May, when the summer monsoon winds begin to sweep across the water[13]. In the northern and southeast Arabian Sea near the west coast of India, the duration of MHWs has increased, leading to more frequent and significantly longer heatwave episodes over the last ten years. Additionally, 2010 and 2016 witnessed the highest number of heat wave days, with heat waves occurring on more than 75 % of days throughout the pre-monsoon and summer monsoon seasons. The present results agrees with those of Gnanaseelan *et al.*[29], who found that high ocean heat content values occurred at 62° E and 10° N during the extreme southwest monsoon. Gupta *et al.*[32] characterised the long-term evolution of MHWs, in both space and time, in the Northern Indian Ocean. Their results revealed that the regimes of MHW intensity and frequency of occurrence exhibit the same spatio-temporal patterns, and that both are showing increasing trends in occurrence, which, in turn, have important consequences for thermal stratification.

The ocean heat content signal amplitudes varied between 0.6×10^9 and 5.8×10^9 J/m^2 and between 3×10^9

and 11×10^9 J/m^2 for the upper 100 m and 300 m layers, respectively. Only in the Arabian Sea, the OHC signal had the greatest value at both layers, because of the temperature difference between the MHWs and the cold upwelling water. This agrees with the conclusion of Maiyza & Mohamed[23]. They showed that there was high amplitude of Sea Surface Temperature Anomaly (SSTA) in the Gulf of Aden and Arabian Sea. In the Equatorial North West Indian Ocean, the OHC signal amplitude was lowest for the upper 100 m layer. For the 300 m layer, several grids had the lowest values (in the Arabian Sea and Indian Ocean at the equator). This lowest annual signal amplitude shows the homogeneity of the water masses in these grids throughout the year.

Conclusion

To conclude, this study computed the ocean heat content patterns and signal amplitudes from the available historical seawater temperature and salinity data in the upper 100 m and 300 m layers of the NWIO. In the upper 100 and 300 m layers, this region, except the Equatorial North West Indian Ocean, displayed the a similar pattern of monthly average ocean heat content. Additionally, throughout the winter and transitional months, the Red Sea's bottom layer displayed a different pattern. The annual amplitude in the NWIO region was found to be uniform, with the Arabian Sea having the largest annual amplitude in both layers. Future research focusing on ocean heat content and its impact on climate change in this region is highly recommended. Also, the investigation of the relationship between ocean heat content and the NWIO region's phenomena, such as the Indian Ocean Dipole, circulation systems, upwelling, and monsoon regimes, is essential.

Conflict of Interest

The authors declare that they have no known competing financial interests or personal relationships that could have appeared to influence the work reported in this paper.

Ethical Statement

This manuscript is authentic, made by the authors themselves, and has not been submitted to another journal or other publishing venue. The four authors have agreed for the submission to the 'Indian Journal of Geo-marine Science', and nominated Prof. Tarek M. El-Geziry as a corresponding author.

Author Contributions

Conception and design of the manuscript: All authors; IAM: Data source; ASD & HIM: Analysis and interpretation of the data; TMG & ASD: Manuscript drafting; IAM, TMG & ASD: Revision of the manuscript. All authors approved the submitted manuscript.

References

1 Banse K & McClain C, Winter blooms of phytoplankton in the Arabian Sea as observed by the Coastal Zone Color Scanner, *Mar Ecol Prog Ser*, 34 (1986) 201-211. https://doi.org/10.3354/meps034201

2 Pham J P, Putting Somali piracy in context, *J Contemp Afr Stud*, 28 (3) (2010) 325-341. https://doi.org/10.1080/02589001.2010.499233

3 Naqvi S W A & Jayakumar D A, Ocean biogeochemistry and atmospheric composition: Significance of the Arabian Sea, *Curr Sci*, 78 (3) (2000) 289-299.

4 Staubwasser M, Sirocko F, Grootes P M & Erlenkeuser H, South Asian monsoon climate change and radiocarbon in the Arabian Sea during early and middle Holocene, *Paleoceanography*, 17 (4) (2002) 1-15. https://doi.org/10.1029/2000PA000608

5 Shankar D, Vinayachandran P N & Unnikrishnan A S, The monsoon currents in the north Indian Ocean, *Prog Oceanogr*, 52 (1) (2002) 63-120. https://doi.org/10.1016/S0079-6611(02)00024-1

6 Naidu P D, Link between western Arabian Sea surface temperature and summer monsoon strength and high-latitude abrupt climate events, *J Geol Soc India*, 68 (3) (2006) 379-385. https://doi.org/10.17491/jgsi/2006/680307

7 Gadgil S & Francis P A, Oceans and the Indian monsoon, In: *Monsoon Monograph*, edited by Tyagi A, Asnani G C, De U S, Hatwar H R & Mazumdar A B, (India Meteorological Department, MoES, GOI), 2012, pp. 129-188.

8 Rajeevan M, Mohapatra M, Unnikrishnan C K, Geetha B, Balachandran S, *et al*., Northeast Monsoon of South Asia, *Meteorol Monogr*, 2 (27) (2022) 1-216.

9 Currie R I, Fisher A E & Hargreaves P M, Arabian Sea upwelling, In: *The Biology of the Indian Ocean*, edited by Zeitzschel B & Gerlach S A, (Springer Berlin, Heidelberg), 1973, pp. 37-52. https://doi.org/10.1007/978-3-642-65468-8

10 Shah P, Sajeev R & Gopika N, Study of upwelling along the west coast of India - A climatological approach, *J Coast Res*, 31 (5) (2015) 1151-1158. https://doi.org/10.2112/JCOASTRES-D-13-00094.1

11 Kämpf J & Chapman P, *Upwelling systems of the world: A scientific journey to the most productive marine ecosystems*, (Springer International Publishing, Switzerland), 2016, pp. 433.

12 Shah P, Sajeev R, Thara K J, George G, Shafeeque M, *et al*., A holistic approach to upwelling and downwelling along the south-west coast of India, *Mar Geod*, 42 (1) (2019) 64-84. https://doi.org/10.1080/01490419.2018.1553805

13 Chatterjee A, Anil G & Shenoy L R, Marine heatwaves in the Arabian Sea, *Ocean Sci*, 18 (3) (2022) 639-657. https://doi.org/10.5194/os-18-639-2022

14 Saranya J S, Roxy M K, Dasgupta P & Anand A, Genesis and trends in marine heatwaves over the tropical Indian Ocean and their interaction with the Indian summer

monsoon, *J Geophys Res Oceans*, 127 (2) (2022) p. e2021JC017427. https://doi.org/10.1029/2021JC017427

15 Maillard C & Soliman G, Hydrography of the Red-Sea and exchanges with the Indian-Ocean in summer, *Oceanol Acta*, 9 (3) (1986) 249-269.

16 Smeed D A, Hydraulic control of three-layer exchange flows: application to the Bab al Mandab, *J Phys Oceanogr*, 30 (10) (2000) 2574-2588. https://doi.org/10.1175/1520-0485(2000)030<2574:HCOTLE>2.0.CO;2

17 Sofianos S S & Johns W E, An oceanic general circulation model (OGCM) investigation of the Red Sea circulation, 1. Exchange between the Red Sea and the Indian Ocean, *J Geophys Res Oceans*, 107 (C11) (2002) 1-17.

18 Campos E J, Gordon A L, Cavalcante G, Kjerfve B & Abouleish M, Impacts of the Red Sea and Persian Gulf on the Northern Indian Ocean in Numerical Simulations, *Ocean Coast Res*, 70 (2022) p. e22050. https://doi.org/10.1590/2675-2824070.22019ejdc

19 You Y & Tomczak M, Thermocline circulation and ventilation in the Indian Ocean derived from water mass analysis, *Deep Sea Res I Oceanogr Res Paper*, 40 (1) (1993) 13-56. https://doi.org/10.1016/0967-0637(93)90052-5

20 Bower A S, Johns W E, Fratantoni D M & Peters H, Equilibration and circulation of Red Sea outflow water in the Western Gulf of Aden, *J Phys Oceanogr*, 35 (11) (2005) 1963-1985.

21 Yao F, *Water mass formation and circulation in the Persian Gulf and water exchange with the Indian Ocean*, Ph.D. thesis, University of Miami, USA, 2008.

22 Bower A S, Hunt H D & Price J F, Character and dynamics of the Red Sea and Persian Gulf outflows, *J Geophys Res Oceans*, 105 (C3) (2000) 6387-6414. https://doi.org/10.1029/1999JC900297

23 Roxy M K, Ritika K, Terray P & Masson S, The curious case of Indian Ocean warming, *J Clim*, 27 (2014) 8501–8509. https://doi.org/10.1175/JCLI-D-14-00471.1

24 Sayantani O & Gnanaseelan C, Tropical Indian Ocean subsurface temperature variability and the forcing mechanisms, *Clim Dyn*, 44 (2015) 2447–2462. https://doi.org/10.1007/s00382-014-2379-y

25 Lee S, Park W, Baringer M O, Gordon A L, Huber B, *et al*., Pacific origin of the abrupt increase in Indian Ocean heat content during the warming hiatus, *Nat Geosci*, 8 (2015) 445–449. https://doi.org/10.1038/ngeo2438

26 Wahiduzzaman M, Cheung K K, Luo J-J & Bhaskaran P K, A spatial model for predicting North Indian Ocean Tropical Cyclone intensity: Role of sea surface temperature and Tropical Cyclone heat potential, *Weather Clim Extrem*, 36 (2022) p. 100431. https://doi.org/10.1016/j.wace.2022.100431

27 Maiyza I A & Mohamed E E, Sea surface temperature anomalies in the northwestern Indian Ocean and its adjacent seas, *Indian J Geo-Mar Sci*, 22 (3) (1993) 180-187.

28 Shi W, Subrahmanyam B & Morrison J M, Estimation of heat and salt storage variability in the Indian Ocean from TOPEX/Poseidon altimetry, *J Geophys Res Oceans*, 108 (C7) (2003) p. 3214. https://doi.org/10.1029/2001JC001244

29 Gnanaseelan C, Chowdary J S, Mishra A K & Salvekar P S, Interannual variability of upper ocean heat content in the northern Indian Ocean, *J Indian Geophys Union*, 7 (4) (2003) 193-200.

30 Vaid B H, Gnanaseelan C, Thompson B, De A & Salvekar P S, Ocean Heat Content variability in the Indian Ocean using Topex/Poseidon Altimeter Data, *J Indian Geophys Union*, 10 (2) (2006) 101-117.

31 Naganamani P V, Ali M M, Goni G J, Udaya Bhaskar T V S, McCreary J P, *et al*., Heat content of the Arabian Sea mini warm pool is increasing, *Atmos Sci Lett*, 17 (1) (2016) 39-42. https://doi.org/10.1002/asl.596

32 Gupta H, Deogharia R, Sil S & Dey D, Characteristics of marine heat extreme evolution in the Northern Indian Ocean, *Int J Climatol*, 45 (2025) p. e8734. https://doi.org/10.1002/joc.8734

33 Mamaev O I, *Temperature – salinity analysis of the World Ocean waters*, (Elsevier Sci Publ, Amsterdam), 1975, pp. 374.

34 Levitus S, Annual cycle of temperature and heat storage in the world ocean, *J Phys Oceanogr*, 14 (4) (1984) 727-746. https://doi.org/10.1175/1520-0485(1984)014<0727:ACOTAH>2.0.CO;2

35 Levitus S, Rate of change of heat storage of the world ocean, *J Phys Oceanogr*, 17 (4) (1987) 518-528. https://doi.org/10.1175/15200485(1987)017<0518:ROCOHS>2.0.CO